Chapter 7
Grain Boundary Segregation and Related Phenomena

Grain boundary segregation affects various physical and chemical properties of the materials, which further control material behaviour. It is mainly the consequence of the close relationship between the grain boundary segregation on the one hand and the grain boundary energy and bonding state on the other hand. The chart listing some metallurgical phenomena affected by grain boundary segregation is shown in Fig. 7.1.

In this chapter, we will present some examples of the effect of grain boundary segregation on material behaviour.

7.1 Grain Boundary Cohesion

Historically, the widely manifested consequence of the grain boundary segregation is its effects on grain boundary cohesion as expressed in a number of well-known forms of intergranular fragility. This continues to provide much of the focus for work in this field. The central problem is the role of solute atoms on atomic cohesion at the interface. As shown in Fig. 7.1, the embrittlement can be of different nature, for example temper embrittlement, hydrogen embrittlement and liquid–metal embrittlement.

7.1.1 Grain Boundary Cohesion and Temper Embrittlement

The majority of the work on grain boundary cohesion has been connected with the effect of additions in iron because of the technological importance of this material [643]. It is now well established that the elements such as copper, zinc, silicon, germanium, tin, phosphorus, arsenic, antimony, bismuth, sulphur, selenium, tellurium, oxygen and manganese all cause intergranular weakness in iron. Similar solutes also weaken copper and nickel. We now consider the two questions (1) why do certain elements weaken the grain boundaries? and (2) what is the relative embrittling potency of these elements? [13].

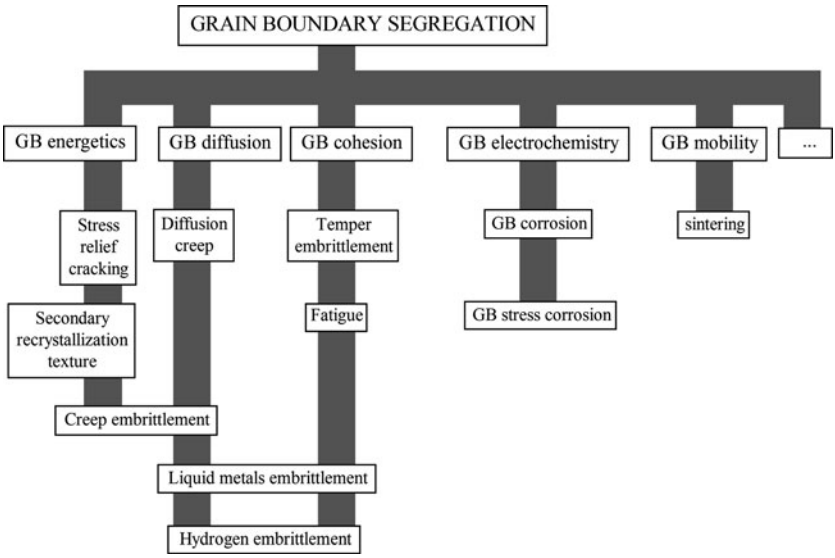

Fig. 7.1 Some materials phenomena influenced by grain boundary segregation (according to [13])

A number of theories have been proposed to account for the role of the solute atoms on grain boundary cohesion. All have a common approach but differ in their interpretation of the way to carry out the numerical calculations. As first, McLean [19] proposed in 1957 that the total work of fracture in low temperature intergranular fracture is the sum of the ideal work of fracture, γ, and the irreversible plastic work of deformation, γ_p. γ is the energy to open the bonds across the interface, and γ_p remains absorbed in the crystal as dislocations and phonons over a region well away from the boundary. γ_p is principally much larger than γ, however, if γ increases, the forces at a crack tip must also be enhanced to propagate the fracture and therefore, γ_p will increase. For a given grain boundary, γ and γ_p are thus directly related. The precise relation will depend on the micro-structure and also on the orientations of the two grains and the grain boundary. The analyses showed that $\gamma_p \propto \gamma^n$ where $n =$ 2–5 [644, 645]. To be able to answer the above questions the effects of segregated solutes on the ideal work of the grain boundary fracture must be understood.

The ideal work of fracture of a non-segregated grain boundary with the energy $\sigma^{\Phi,0}$ is [19]

$$\gamma^0 = 2\sigma^{s,0} - \sigma^{\Phi,0}, \tag{7.1}$$

where $\sigma^{s,0}$ is the surface energy of the pure material because by opening the grain boundary two free surfaces are created. An analysis of the values of $\sigma^{s,0}$ and $\sigma^{\Phi,0}$ for many metals shows that typically, $\sigma^{\Phi,0} \approx \sigma^{s,0}/3$ [371]. Accordingly, the ideal work of fracture of the pure grain boundaries is only slightly lower than that of an average plane in the crystal (approximately 5/6 of it). It does not mean automatically that the grain boundaries will always fail in preference to cleavage. The fracture manner will also depend on the orientation of the slip planes and the surface energy of the

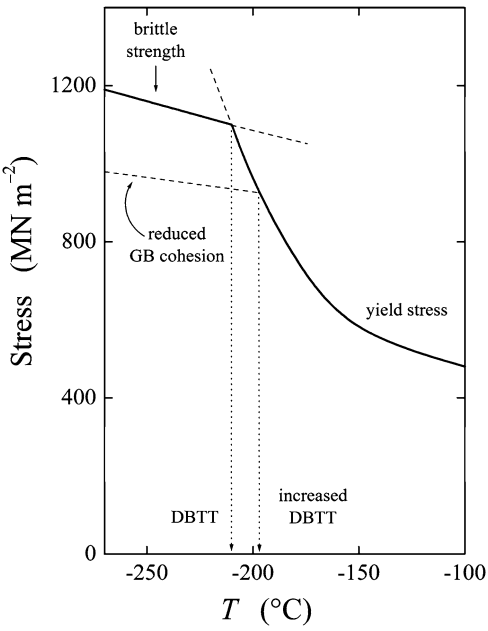

Fig. 7.2 Schematic representation of the increase of the DBTT as a result of reduced grain boundary cohesion due to solute segregation in a 0.2% carbon steel (according to [13, 647])

low-index cleavage planes makes cleavage generally more likely than intergranular failure in clean bcc metals [646].

Let us comment now the balance between brittle and ductile failure. For example, the fracture behaviour of a 0.2% carbon steel is shown schematically in Fig. 7.2 in dependence on the test temperature [13, 647]. At high temperatures, the dislocations move easily and the yield stress is low. Therefore, the steel fails in a ductile manner. At lower temperatures, the dislocation movement becomes more difficult and the material eventually fails in a brittle manner. The highest temperature at which this occurs is the ductile–brittle transition temperature (DBTT). Sometimes, DBTT is also called as the fracture appearance transition temperature (FATT) or the onset of the upper shelf transition (OUST) [47]. The temperature dependence of the fracture energy is schematically depicted in Fig. 7.3. The DBTT corresponds to the inflection point of this dependence.

Solute segregation at the grain boundaries may lead to a sufficient reduction of the grain boundary cohesion and therefore, DBTT is increased so that the otherwise ductile material becomes brittle.

A thorough thermodynamic analysis of the ideal work of fracture of segregated grain boundaries, γ, has been made by Hirth and Rice [648]. According to their theory, the reduction of the ideal work of fracture if there is no redistribution of the

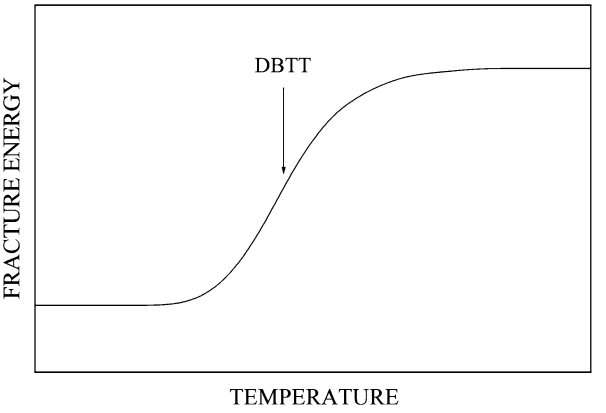

Fig. 7.3 Schematic course of the temperature dependence of fracture energy defining the DBTT

segregated species is given by

$$\gamma = \gamma^0 - \int_0^{\Gamma_I^\Phi} \left[\mu_I^\Phi(\Gamma) - \mu_I^s(\Gamma/2)\right] \mathrm{d}\Gamma, \tag{7.2}$$

where μ_I^Φ and μ_I^s are the grain boundary and surface chemical potentials of solute I in equilibrium with a level of the grain boundary adsorption, Γ_I^Φ. This expression can be written as

$$\gamma = \gamma^0 + \Gamma_I^\Phi \left(\Delta G_I^s - \Delta G_I^\Phi\right) + RT \int_0^{\Gamma_I^\Phi} \ln \frac{\Gamma_{I,\max}^\Phi - \Gamma}{\Gamma_{I,\max}^s - \Gamma} \mathrm{d}\Gamma, \tag{7.3}$$

where $\Gamma_{I,\max}^\Phi$ and $\Gamma_{I,\max}^s$ are the maximum adsorption levels at the boundary and surface, respectively. ΔG_I^s and ΔG_I^Φ are the Gibbs energies of segregation of solute I at the surface and at the grain boundary, respectively [649]. In the dilute limit, the last term on the right-hand side of (7.3) equals to $-RT$ ln2 and usually, it can be neglected (RT ln2 = 5.76 kJ/mol at 1,000 K). The ideal work of fracture thus decreases linearly with the level of segregation, and those elements that segregate more strongly to free surfaces than to grain boundaries reduce the ideal work of fracture and vice versa. Equation (7.3) also suggests the change of the DBTT with segregation, $\partial \mathrm{DBTT}/\partial \Gamma_I^\Phi \propto \left(\Delta G_I^s - \Delta G_I^\Phi\right)$ [366]. Measurements of ΔH_I^s, ΔH_I^Φ and Γ_I^Φ in Ni_3Al bicrystals containing the artificial cavities at the grain boundary performed by Otterbein et al. showed the decrease of the grain boundary cohesion caused by sulphur segregation [650]. Similarly, the reduction of the cohesion energy of the {013} symmetrical tilt grain boundary by 56.4 mJ/m^2 (i.e. by 1.5 rel.%) was caused by complex segregation of silicon, phosphorus and sulphur in an Fe−Si alloy [651].

An alternative approach of Seah [652] giving the same result in the quasi-chemical pair bonding approximation is based on evaluation of the actual bond energies across the boundary before and after fracture,

$$\gamma = \gamma^0 + \Gamma_I^{\Phi} \left(\frac{Z_g}{Z \Gamma_I^{\Phi,0}} \right) \left(H_I^{\text{sub},*} - H_M^{\text{sub},*} - \frac{Z\Omega}{a_I^2} \right), \tag{7.4}$$

where $\Omega = H_{\text{mix}}/[ZX_I(1-X_c)]$ with the mixing enthalpy, H_{mix}. Z_g is co-ordination number at the grain boundary, Z is the bulk co-ordination number and $H_{I,M}^{\text{sub},*}$ are the sublimation enthalpies of solute I and matrix element M. $\Gamma_I^{\Phi,0}$ is the value of Γ_I^{Φ} at one monolayer and a_I is the atomic diameter of the segregated solute atom. In the regular solution approximation when Ω is neglected, the lower the value of $H_I^{\text{sub},*}$, comparing to that of the matrix element, the more will a segregated solute embrittle its grain boundaries. Figure 7.4 summarises the values of $H_I^{\text{sub},*}$ for numerous elements and clearly indicates that the solutes such as antimony, tin, sulphur, phosphorus, manganese, silicon and copper, with the values of $H_I^{\text{sub},*} < H_{\text{Fe}}^{\text{sub},*}$ below the limit represented by the dashed horizontal line, will all embrittle iron. On the other hand, the solutes with higher values of $H_I^{\text{sub},*}$ such as molybdenum and carbon, will improve the cohesion as was also confirmed experimentally [13].

There is numerous experimental evidence that the chart in Fig. 7.4 is generally valid for other materials than iron. For example, carbon increases the grain boundary cohesion of molybdenum and tungsten, but the effect of oxygen is quite opposite [653, 654], segregations of silicon and thorium reduce the grain boundary cohesion of iridium [389], lithium reduces the cohesion of aluminium [655] but boron segregation strengthens grain boundaries of Ni_3Al [656] and copper [657].

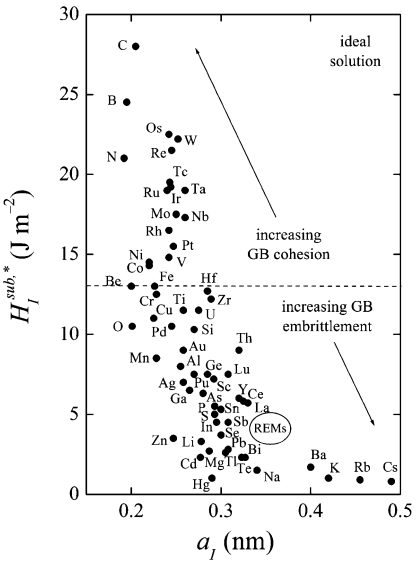

Fig. 7.4 The plot of the sublimation enthalpy, $H_I^{\text{sub},*}$, vs. lattice parameter of the corresponding solute, a_I. The elements having the value of $H_I^{\text{sub},*}$ higher than any chosen matrix element (for example iron as suggested by the dashed horizontal line) increase its ductility while those with lower value of $H_I^{\text{sub},*}$ embrittle the matrix (according to [19, 652])

However, exclusive consideration of the effect of segregated solutes on the ideal work of fracture is not sufficient. One must keep in mind that there is a choice between dislocation emission and bond breaking at a crack tip that decides whether ductile cleavage or brittle fracture occurs. It can be shown that the segregated solutes causing the embrittlement increase the ease of dislocation emission at the crack tip, so offsetting the total embrittling effect discussed above. The correction is small but allows the correct prediction of the absolute embrittlement of cooper by bismuth [658].

A thorough study of the structure and solute effects on grain boundary fracture was performed on molybdenum [659]. It was shown that low angle and twist grain boundaries are strong but the majority of the interfaces are weak. It indicates an intrinsic brittleness of the grain boundaries due to the interatomic bonding of molybdenum. The weak grain boundaries can be strengthened by segregation of interstitial impurities such as carbon or nitrogen. In the latter case, a weak strengthening effect is due to precipitation of grain boundary nitride [659].

The aspects of chemical bonding in grain boundary segregation can be elucidated by ab initio calculations of chemical bonding in clusters with the same atomic arrangements as these in the structural units of a grain boundary (polyhedral structures). Application of the molecular orbital method on tetrahedral Me_4I clusters to segregation of sulphur and boron at grain boundaries of nickel and iron as well as of segregation of carbon in iron revealed a redistribution of electron charge density in the grain boundary [503, 660, 661]. In case of electronegative sulphur, the charge is drawn from the surrounding metal atoms to that of sulphur and – consequently – the adjacent metal–metal bonds are weakened [660, 662]. The bonding parallel to the boundary is stronger than perpendicular one, and therefore, the cohesion across the boundary is reduced and grain boundary embrittlement results [663]. Qualitatively similar charge transfer was calculated for the case of phosphorus in bcc iron [664]. Strong bonding orbitals are formed between Fe(3d) and P(3p) orbitals in Fe_xP clusters at the grain boundaries, and thus, the metallic bonds between Fe_xP clusters and surrounding Fe atoms are weakened, which give rise to embrittlement [258]. The average d-band energy is higher with phosphorus (and also sulphur) than in pure metal. Then, more antibonding states are filled and cohesion is reduced [665]. In case of the less electronegative atoms of boron and carbon, relatively strong covalent-like bonds form with metal in direction perpendicular to the boundary, whereas much weaker bonding occurs in parallel direction. This kind of bonding enhances grain boundary cohesion [257, 258, 260, 662, 664]. In contrast, boron atoms occupy positions in the centre of compact polyhedra of iron atoms with little change in the structure of iron grain boundary. Therefore, the stress field is not changed by boron segregation [546], but weaker bonds in the iron grain boundary are strengthened due to the interaction of bulk dislocations with segregated atoms at the boundary [666]. Addition of boron to iron containing phosphorus evokes a site competition at the grain boundaries and phosphorus atoms are replaced by boron ones. Consequently, the material exhibits improved grain boundary ductility due to this "cleansing" effect of site competition [276]. Boron and carbon reduce the average d-band energy for the neighbouring iron atoms, fewer antibonding states are

thus filled and cohesion increases [665]. Other elements such as nitrogen exhibit the bonds with some ionic character. This may be an important reason of nitrogen behaving differently from phosphorus [667]. In case of a more complex system with the grain boundary segregation of titanium, boron and oxygen, co-segregation of titanium and boron, both of which enhance grain boundary cohesion of iron, increases the cohesion. If titanium co-segregates with oxygen, the embrittling effect of the latter solute is completely reduced [668].

Similar situation occurs in Ni−S system [661]. As sulphur segregates at the grain boundaries of nickel, both the cohesive strength in vicinity of the segregated atom and the shear strength are reduced. Overcoming a critical grain boundary concentration, the network of S−S bonds within a grain boundary is formed. As a consequence, the shear stress begins to increase but the cohesive strength continues to reduce so that the conditions for brittle fracture are fulfilled. If a different solute such as boron segregates, no apparent decrease of the cohesive strength occurs [669]. Boron forms similarly strong bonds with nickel as sulphur, however, the valence orbitals of boron are compact because large ion core is absent in contrast to those of sulphur that are more extended. As a result, boron forms bonds at smaller hole sites with less intrinsic strain comparing to sulphur. Consequently, the metal–metal bond is weakened in vicinity of sulphur atoms in contrast to the case of boron, which needs less additional strain [668].

The effect of sulphur on reduced cohesion can also be explained by repulsive interaction between sulphur atoms in nickel resulting in prolongation of S−S bonds and to a consequent interfacial decohesion [670]. Another explanation for the sulphur-induced decohesion of nickel is based on consideration of directional change of chemical bonding [671]: The question of the true mechanism of the decohesion remains still open [672]. Similarly to sulphur, other metalloids are reported to reduce usually the grain boundary cohesion except beryllium, boron, carbon and silicon while aluminium and phosphorus are indicated as indifferent to nickel embrittlement [673]. This result seems not to agree completely with the results of Seah and Hondros [13, 652] (Fig. 7.4) according to which beryllium and silicon as well as phosphorus and aluminium should also be grain boundary embrittlers. This discrepancy may be affected by the fact that the calculations were performed for the $\Sigma = 5, \{012\}$ special grain boundary with principally low segregation energy.

The charge changes induced by solute segregation are probably the reason for grain boundary embrittlement of aluminium by gallium. First-principles pseudopotential calculations showed that gallium at the grain boundary in aluminium draws charge from the surrounding matrix atoms as a result of the difference in electronegativity between these two elements. As a result, the charge density is reduced between gallium and aluminium atoms as well as between aluminium atoms along the grain boundary [255].

Besides the case of sulphur embrittlement of nickel [670–672], a heavy discussion concerns the effect of bismuth on intergranular embrittlement of copper. A redistribution of the charge density due to grain boundary segregation of bismuth in copper was described to directly weaken the bonds between dissimilar atoms in Cu_6Bi grain boundary clusters [674]. There exist three models for bismuth

embrittlement of copper. Two models are based on changing electronic structure (a) the strengthening of the bonds of the surrounding metal by bismuth and thereby inhibiting the bond mobility that is a necessary condition for plasticity [675], and (b) the weakening of the bonds across the GB by bismuth [668]. These models assume that the weakening is an electronic effect, where the more electronegative segregated atom withdraws electrons from the metal d-bands thus reducing the bond strength. This interpretation is based on electron microscopic observation of the "white lines" in the inelastic electron scattering intensity observed at bismuth segregated grain boundaries of copper. Recently, the role of the electronic effect was supported when almost no expansion was found at the 36.9°[001], {310} symmetrical tilt grain boundary segregated by bismuth [674]. The embrittlement was attributed to an electronic effect: the Cu d-band retreats below the Fermi level, reducing sd hybridisation. However, it is not clear whether the grain boundary was embrittled either in the calculations or in the measurements. In addition, the grain boundary concentration of bismuth observed in this case 2.9 at/nm^2 is about 5 times lower than measured at grain boundaries [676]. The electronic effect is rather small in this case and cannot account for the reduction of fracture toughness. Let us add that sodium should also be a good embrittler of copper albeit silver acts as a modest cohesion enhancer [677].

The third model for embrittlement of copper due to the grain boundary segregation of bismuth is a size effect suggested by Sutton and Vitek [545]. This model is based on two necessary conditions for copper embrittlement due to grain boundary segregation: The solute is virtually insoluble and has much larger atomic radius than the matrix element. The solute then segregates to the boundary thus pushing apart copper atoms across the interface and weakening the interatomic bonding. The first-principles quantum-mechanical calculations [261] support the latter model. In addition, the size effect seems also to be responsible for copper embrittlement induced by lead and mercury segregation: The latter two solutes are practically indistinguishable in the properties contrary to the expectations following from the models of changing electronic structure [678].

The results of computer simulations proved that the grain boundary structure also plays an important role in the fracture properties of brittle materials [679]. For example, low energy fracture was observed at room temperature for the high-angle grain boundaries of molybdenum containing traces of oxygen and carbon. This behaviour was observed for the [100] symmetrical tilt grain boundaries with the misorientation angles 20°, 30°, 50°, 52° and 70°. On the other hand, high energy is necessary to fracture the boundaries misoriented by 5°,10° and 88° [680]. This behaviour very probably reflects the level of carbon and oxygen segregation at high angle grain boundaries [653]. Similar results were observed for tungsten [654].

The structure of the grain boundaries in conjunction with corresponding solute segregation also affects strongly the fracture characteristics. Recently, the role of the grain boundary plane orientation in the segregation-induced embrittlement was studied in case of bismuth segregation in copper [681]. Both experimental and theoretical studies of the asymmetrical tilt grain boundaries in the $\Sigma = 9$ [110] showed that highly segregated general grain boundaries exhibit brittle intergranular fracture

while in case of the special ones containing low level of bismuth segregation, the transgranular ductile fracture is observed. It is interesting to note that the special grain boundaries are characterised by {111}, {112} and {114} planes on one side of the grain boundary [681].

Another approach to the problem of grain boundary embrittlement is based on direct consideration of impurity–impurity bonds [682]. Particularly, the effect of formation of covalent *I–M–I* bonds on material embrittlement depends on the type and valence of impurity I. For example, sulphur needs two electrons to complete its 3p-subshell so that it will form two bonds at a nickel boundary. One of these bonds is parallel and the other perpendicular to the boundary. The redistribution of the metal charge will then occur preferentially into bonds parallel to the grain boundary. The energy difference between the two types of the bonds then determines the embrittling potency of the segregated elements: in the case of sulphur an embrittlement occurs. On the other hand, boron with only one p-electron forms only bonds across the interface so that the charge flow exists in this direction: in this case, no embrittlement occurs.

7.1.2 Hydrogen Embrittlement

Another effect, which reduces the grain boundary cohesion, is hydrogen embrittlement. This effect has received a considerable interest during past decades, because hydrogen is present in the environment [683]. Absorbed hydrogen atoms preferentially segregate at the micro-crack surface along the grain boundaries thus increasing the stress ahead its tip. It is possible that some hydrogen atoms also recombine to molecules and the stress at the micro-crack tip is further enhanced although this effect is probably not so large. As a result of these stresses, micro-cracks grow and form micro-cavities. Segregated hydrogen can possibly cause two different situations, dislocation-screened tips and dislocation-assisted crack tips [638].

The microscopic model of hydrogen embrittlement starts from a hydrogenated elastic–plastic material with a crack embedded along the grain boundary. The crack tip is screened by dislocations. Under stressing this body, the crack is loaded in the direction perpendicular to the crack plane by a remote applied stress. The dislocation-screened crack preserves a local stress in the dislocation-free zone and produces a stress intensity. The crack tip can maintain a local equilibrium expressed as [638]

$$\varphi = \cos^{-1}\left(\frac{\gamma^{\Phi}}{2\gamma^{\mathrm{s}}}\right), \tag{7.5}$$

where ϕ is the half crack-tip angle, γ^{Φ} and γ^{s} are the grain boundary and the crack surface energy, respectively. At the grain boundaries, the equilibrium hydrogen segregation should then occur. Since this segregation at the crack surfaces and grain boundaries affects both γ^{Φ} and γ^{s}, the crack tip profile, the local stress and the ideal work change. Eventually, the relationship for theoretical stress-intensity factor, $K^{\mathrm{c}}_{\mathrm{th}}$,

can be derived from the local energy balance,

$$K_{\mathrm{th}}^{\mathrm{c}} = K_0 \left(\frac{\gamma}{2\gamma_0} \right)^{[(n+1)/4n]} \left[\frac{\tan(\varphi_0/2)}{\tan(\varphi/2)} \right]^{[(1-n)/4n]}, \tag{7.6}$$

where n is the work hardening coefficient, the index 0 indicates the quantities in the absence of hydrogen segregation. The dependence of $K_{\mathrm{th}}^{\mathrm{c}}$ on the bulk concentration of hydrogen is the function of the energy of the hydrogen binding at the crack surfaces and the grain boundaries as well as plastic deformation characterised by the parameter n and the yield stress [638].

Latanision and Opperhauser [684] showed that the segregated solutes at the grain boundary reduce the recombination of hydrogen atoms and promote penetration of hydrogen along the grain boundaries. These solutes, such as phosphorus, sulphur, arsenic and antimony, which have a strong tendency to segregate to grain boundaries in steel, have also a stronger intrinsic binding to hydrogen than iron [685, 686]. Hydrogen atoms, which dissociated from molecules adsorbed from the vapour or from solution, bond strongly with the segregated atoms and reside at the grain boundary sites much longer than at the single ones. Consequently, there is a greater chance for hydrogen to be absorbed into the lattice. Therefore, the role of these segregated solutes consists in increasing the amount of hydrogen trapped in the grain boundary core. If the mechanism of hydrogen-embrittlement requires the concentration of hydrogen in the metal just ahead of the crack tip, the above solutes segregated at the grain boundary should therefore aid this embrittlement [13]. Kameda and McMahon detected the first intergranular micro-cracks induced by hydrogen in antimony doped Ni–Cr steel using acoustic emission and obtained corresponding threshold stress for its onset. This stress depends on the grain boundary segregation of antimony. Once the threshold stress is reached, the crack spreads and the decohesion occurs [687]. Similarly, grain boundary segregation of phosphorus and sulphur assists to hydrogen embrittlement of an X–750 nickel-based superalloy. Occurred micro-cracks can then facilitate stress corrosion cracking in water environment [688].

As expected, hydrogen serves at the grain boundaries of iron as electron acceptor and the H–Fe bonding is rather ion-like than covalent but strong. Presence of hydrogen thus leads to a similar reduction of the charge density in the region between iron atoms across the grain boundary as in case of other metalloid impurities. The charge transfer from Fe to H at both the grain boundary and free surface seems to be the key mechanism for hydrogen embrittlement [689]. In fact, hydrogen atoms are extremely mobile and their segregation is not expected to be too large. The main role of hydrogen in intergranular embrittlement consists in nucleation of the cracks rather than in their spreading [690] due to its dynamic effect occurring in course of loading the sample.

The reduced cohesion of the grain boundaries resulting from hydrogen segregation (hydrogen embrittlement) is sometimes used to facilitate intergranular fracture of less segregated or less brittle grain boundaries for studies of grain boundary segregation by the techniques of surface analysis such as AES [683]. In case of a 7050

aluminium-based alloy, magnesium segregation reduces the cohesion of the grain boundaries, while the opposite effect is observed for segregation of copper [691].

Recent study of the hydrogen-induced cracking in high-purity high-strength 4340 type steel showed that elimination of embrittling impurities does not eliminate the susceptibility of this material to hydrogen embrittlement under high yield strength if the strain rate is small enough [692].

7.1.3 Other Types of Non-reactive Environmental Decohesion

Hydrogen is typical example of intergranular decohesion of polycrystalline materials caused by the impurity atoms localised at the grain boundaries. Similar effect was observed when liquid metal penetrates along the grain boundaries into the material volume (liquid metal embrittlement (LME)) or by penetration of the atoms adsorbed at the surface (either from the environment or from the material volume) to the free surface in the grain boundary micro-cracks (dynamic embrittlement). Let us briefly touch both these effects.

7.1.3.1 Liquid Metal Embrittlement

Presence of a liquid metal on the surface of a polycrystalline material may be dangerous for its integrity because the liquid metal may penetrate along the grain boundaries and reduce substantially their cohesion. Classical example of this LME is the grain boundary penetration of mercury to β-brass at room temperature [7]. Other examples are listed in Table 7.1.

LME can have very dangerous consequences for service of some metallic parts of the machines. Quite frequently, this problem is observed in case of rotating parts of the gas turbines. A wide intergranular degradation was observed in case of a turbine rotor bolt made of IN 718, UNS N07718 after its service operation at about 540°C. High level of cadmium at the fracture surfaces indicated that this element present in cadmium-rich smear on the treated flank was melted (melting point of cadmium is 321°C) and penetrated quickly along the grain boundaries into the rotor bolt [693].

Table 7.1 Metals exhibiting LME. According to [47]

Matrix	Embrittling solute
Fe	Bi, Pb, Sn, Zn
Zn	Bi, Cd, Ga, Hg, In, Sn
Cu	Bi, Cd, Hg, In, Pb
Al	Cd, Ga, Hg, In, Na, Sn, Zn,
Ag	Ga, Hg
Cd	Ga, In, Sn
β-brass	Hg

Similarly to other interfacial phenomena, LME is anisotropic, that is its velocity depends on the grain boundary structure. Kargol and Albright [694] showed that the $\Sigma = 3, 70°[110]$ and $\Sigma = 11, 130°[110]$ grain boundaries in aluminium are highly resistant to LME compared to other [110] characterised interfaces. Detailed study of structural dependence of fracture stress of zinc bicrystals deformed under effect of liquid gallium showed maximum resistance of the $\Sigma = 9, 56.6°[10\bar{1}0]$ grain boundary [695]. In polycrystalline bcc β-brass, the cracks of LME were nucleated and propagated preferentially at general grain boundaries [696].

Grain boundary segregation of some impurities can significantly enhance the susceptibility of the material to LME. For example, tin and antimony segregation in steel increase the LME by lead while it is reduced under phosphorus and arsenic segregation [47, 697]. Increased phosphorus segregation also reduces intergranular embrittlement of Monel 400 LME by mercury [698] and tin segregation at copper grain boundaries – although it does not cause materials embrittlement itself – increases susceptibility of copper to LME by mercury [699].

A special case of the LME is the grain boundary wetting resulting in grain boundary phase transitions (e.g. [72]). In this case the liquid metal may penetrate very quickly along the grain boundaries causing their "melting" and thus loss of cohesion. As examples of this effect, we can mention the grain boundary wetting in systems Al−Sn [700], Zn−Sn [701], Cu−In [702] or (Fe−Si)–Zn [703]. Here, we will not discuss this problem, but we refer to special publications in this field (e.g. [72]).

7.1.3.2 Dynamic Embrittlement

In contrast to the low-temperature intergranular damage caused by equilibrium segregation and sudden brittle fracture, a relatively slow, stepwise brittle intergranular decohesion process can occur at enhanced temperatures in some materials under stress or when they are stressed in a specific environment. This process is called *stress-relief cracking* or *dynamic embrittlement* [704–706]. The mechanism of this process is controlled by adsorption of specific atoms at the free surface of the crack tip under external loading. Thus, the cohesion of the grain boundary changes and may result in cracking of the grain boundary bond closest to the surface in the crack tip. The atoms then adsorb again at the surface of the crack tip and the process of decohesion continues. The diffusive nature of this penetration controls the process, and therefore, the crack propagation is relatively slow [707]. The source of the embrittling element can be either external (adsorption from the environment) or internal (surface segregation from the material volume) [708].

The dynamic embrittlement can be described on basis of combined diffusion and straining processes. The unidirectional flux of atoms I along the grain boundary, J_I, due to the stress-induced potential gradient under diffusion is [709]

$$J_I = -D_I^{\Phi}\frac{\partial X_I^{\Phi}}{\partial x} + \left(\frac{D_I^{\Phi} X_I^{\Phi} \Omega_I^{\Phi}}{kT}\frac{\partial \sigma}{\partial x}\right) + \left[\frac{D_I^{\Phi} X_I^{\Phi}\left(1 - X_I^{\Phi}\right)}{kT}\left(\varphi_M(\delta) - \varphi_I'(\delta)\right)\frac{\partial \delta}{\partial x}\right], \tag{7.7}$$

where the gradient of the chemical potential, $\nabla\mu_I^\Phi = \Omega_I^\Phi \nabla\sigma$, Ω_I^Φ is the atom volume of I and $\nabla\sigma$ is the relevant stress gradient, D_I^Φ and X_I^Φ are the grain boundary diffusivity and the concentration of I, respectively, δ is the grain boundary thickness and ϕ_J ($J = I, M$) are the interfacial "cohesive functions" of pure I and M interfaces. The continuity equation with constant D_I^Φ provides [709]

$$\frac{\partial X_I^\Phi}{\partial t} = D_I^\Phi \frac{\partial^2 X_I^\Phi}{\partial x^2} - \frac{D_I^\Phi \Omega_I^\Phi}{kT}\left(\frac{\partial X_I^\Phi}{\partial x}\frac{\partial \sigma}{\partial x}\right) - \frac{D_I^\Phi}{kT}\left[\frac{\partial\left(X_I^\Phi\left(1 - X_I^\Phi\right)\right)}{\partial x}\left(\varphi_M(\delta) - \varphi_I'(\delta)\right)\frac{\partial^2 \delta}{\partial x^2}\right], \tag{7.8}$$

where suffix Φ relates the variable/parameter to the grain boundary [709]. The kinetic parameter relating the diffusion and deformation rate, $\Re$, is under bulk diffusion control

$$\Re = \frac{t_\mathrm{d}}{t_\mathrm{r}} = \frac{\dot{a}\delta_\mathrm{c}^2}{D_I(\delta_\mathrm{c} - \delta_0)} \tag{7.9}$$

where t_d and t_r are the characteristic diffusion time and the time to rupture, δ_c and δ are the critical and equilibrium separation distances, respectively, and $\dot{a}$ is the separation rate [707].

The dynamic embrittlement was observed in numerous systems, for example in bicrystals of Cu−Sn alloys in vacuum [710], polycrystalline IN 718 nickel-based superalloy [711], MnMoNiCr steel [712], Ni_3Al [713] and Cu−Be alloy [714] in air.

Similarly to other examples of material embrittlement, dynamic embrittlement is also sensitive to grain boundary structure. As a result, the resistance of the material against dynamic embrittlement increases with increasing frequency of special grain boundaries (cf. Sect. 7.4). Oxygen-induced dynamic embrittlement of IN 718 nickel-based superalloy showed that general and/or the less coincident grain boundaries crack easily than the $\Sigma = 3$ and $\Sigma = 5$ grain boundaries although neither this boundary nor the low-angle interfaces are completely immune from cracking [708, 715].

7.2 Grain Boundary Corrosion

Since the grain boundaries are regions of enhanced energy, they are prone to localised corrosion. This is the basis for visualisation of the grain structure by chemical etching of polycrystalline samples in specific agents or by thermal etching during vacuum annealing. The corrosion attack can be accelerated or sometimes completely induced by stressing the material in aggressive environment resulting in intergranular brittle degradation of the material. In such case, the stress-corrosion cracking occurs. In the present part, we will discuss the pure corrosion and stress-corrosion cracking of the materials.

7.2.1 Corrosion

During chemical or thermal etching, the grain boundaries are attacked and the grooves are formed. If the period of the attack is long enough, polycrystalline material can be completely separated along the grain boundaries in the absence of applied stress. The mechanism of this environmentally assisted cracking is preferential attack of grain boundaries outcoming to a non-protected surface. The crack then propagates into the material along the grain boundaries due to electrochemical processes (e.g. anodic dissolution) [47]. Grain boundary segregation can play an important role in promoting this process in various ways. Either, a less noble layer is formed at the segregated grain boundary which is more prone to the above-mentioned dissolution (e.g. copper in silver, see below), or a segregated element can react with another one and change the anticorrosive ability of the grain boundary such as carbon with chromium in austenitic stainless steels [47].

Due to the anisotropy of grain boundary energy and segregation, there also exists the orientation dependence of intergranular corrosion. For example, minima of the penetration depth or the width of the etched boundary groove corresponding to the minima of the measured boundary energy were found at certain [100] tilt grain boundaries in aluminium [57, 716], Cr−Ni austenitic stainless steel [717], niobium [718] and copper and α-Cu−Al alloy [719]. Low values of the etch groove depth were also found at the low-Σ grain boundaries in a polycrystalline Fe−Ni−Cr alloy [529, 720]. It was shown that a special etching agent containing picric acid as an active component attacks only the austenitic grain boundaries in a Ni−Cr steel that were segregated by phosphorus [721]. The treatment of polycrystalline stabilised 310 stainless steel in boiling nitric acid revealed the highest corrosion resistance of the $\Sigma = 3$, $\Sigma = 11$ and $\Sigma = 13$ grain boundaries [722]. Surprisingly, the maxima of the penetration depth were reported for the low energy {013}, {012} and {023} symmetrical tilt grain boundaries in a 17Cr−13Ni austenitic stainless steel containing silicon [533]. The orientation dependence of the penetration depth copies analogous dependence of the level of silicon segregation at individual grain boundaries for both 0.3 and 0.8mass.% of silicon in the bulk. The differences in corrosion behaviour of both symmetrical and asymmetrical tilt grain boundaries in one sample were studied on curved grain boundaries corresponding to 36.9°[100] and 45°[100] orientation relationships [87, 723]. As it is apparent in Fig. 7.5a, the width, w, of the etched groove changes with the grain boundary inclination. There exist two minima of w at the inclinations 18.5° and 26.5° from original {013} grain boundary corresponding to the (001)/(034) and (011)/(017) asymmetrical grain boundaries, respectively (Fig. 7.5b) [723]. This finding is in very good agreement with the orientation dependence of the standard enthalpy of solute segregation (Fig. 5.16), and with the finding that the (011)/(017) asymmetrical grain boundary is special and the (001)/(034) one exhibits vicinal behaviour [94, 95]. Similarly, a single minimum of w was found at the curved 45°[100] grain boundary corresponding to the special (001)/(011) grain boundary [87, 94, 95].

Another interesting example of anisotropic interfacial corrosion can be shown in case of the archaeological buried objects. The necklace of a Ag−1mass%Cu−0.3mass.%Au alloy, excavated from a grave and dated to the tenth century, exhibited

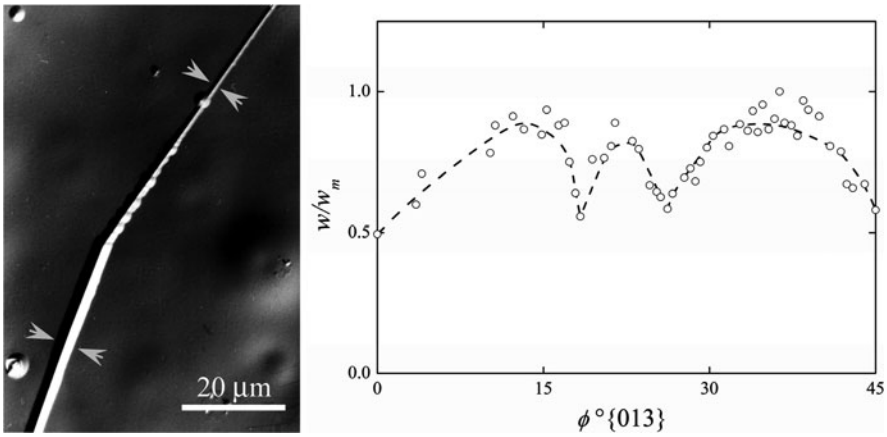

Fig. 7.5 Corrosion of the curved 36.9°[100] grain boundary (**a**) micro-structure of the etched grove in Nomarski interference contrast (conical objects on the grain surfaces are dislocation etch pits); (**b**) orientation dependence of its width, w, normalised by the maximum value of the width, w_{m} (according to [723])

an extended intergranular brittle failure [724]. The analysis of the parts of this necklace proved that this failure is caused by intergranular corrosion of less noble copper-segregated grain boundary regions under the conditions of decomposing human body. A thorough crystallographic investigation proved that all failed grain boundaries were non-coincidence and no separation was observed along the low-Σ grain boundary. In addition, about 20% of non-coincidence grain boundaries were also found to be resistant to the corrosion attack. Some of these boundaries were surrounded exclusively by special twin boundaries preventing penetration of the electrolyte to them. However, some non-coincidence grain boundaries were found to be resistant to the corrosion although they were in contact to the strongly corroded interfaces. This is the case of the grain boundaries with the surface traces characterised by the ⟨126⟩/⟨011⟩ and ⟨112⟩/⟨237⟩ directions measured in respect to the adjoined grains parallel to the two respective grain boundaries (Fig. 7.6). These interfaces are joined with another non-coincidence grain boundaries characterised as ⟨115⟩/⟨035⟩, and ⟨116⟩/⟨023⟩ directions, that are heavily corroded.

We may deduce the character of these grain boundaries by accounting for the orientations of the planes belonging to the crystallographic zones of these directions. The crystallographic zones corresponding to at least one of the measured directions of both resistant grain boundaries, ⟨011⟩ and ⟨112⟩, can lay in the densest plane of the {111} type. On the other hand, the ⟨115⟩, ⟨035⟩, ⟨116⟩ and ⟨023⟩ directions of the corroded grain boundaries cannot lay in the {111} type plane. It is highly probable from energetic reasons that the untouched ⟨126⟩/⟨011⟩ and ⟨112⟩/⟨237⟩ grain boundaries in Fig. 7.6 are formed by the planes of the {111} type. This deduction follows our model of classification of grain boundaries in bcc iron according to which

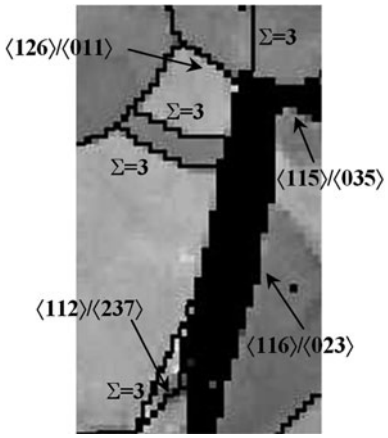

Fig. 7.6 Example of resistant and corroded non-coincidence grain boundaries. The Miller symbols give the directions parallel to the grain boundary plane in respect to both adjoining grains [724]

there exists special asymmetrical tilt grain boundaries formed by the bcc densest {110} plane on one side [91, 94]. It is highly probable that the grain boundaries formed by the {111} fcc densest planes are special [94, 724].

7.2.2 Stress Corrosion Cracking

Simultaneous effect of corrosive environment and stressing the sample with a susceptible micro-structure can often result in brittle fracture also in case of the materials ductile under acting these effects separately. This phenomenon is called *stress corrosion cracking*. Stress corrosion cracking can pass transgranularly as well as intergranularly. Intergranular stress corrosion cracking is more frequent and also more dangerous for the behaviour of the parts in service [725], mainly in case of austenitic stainless steels in commercial boiling water reactor nuclear power plants [726].

Grain boundaries play an important role in localised corrosion as mentioned in the previous part. It is obvious that – similarly to simple corrosion – the grain boundary structure and dominantly its chemistry will also affect the course of intergranular stress corrosion cracking [725]. The initiation of the cracks during the stress corrosion is closely related to (a) the activated dislocation slip system, (b) the grain misorientation, (c) the misorientation of the Burgers vectors of the primary slip systems and the grain boundary plane and (d) the deformation behaviour in vicinity of the grain boundary [727]. Room-temperature intergranular stress corrosion cracking studied thoroughly in bicrystals of an α-Cu−9at.%Al alloy containing specific [100] and [110] tilt grain boundaries in solution of NH_4OH and NaOH under constant stresses in range of 0.8–2 related to the yield stress of the material was found to exhibit a pronounced anisotropy. The susceptibility minima of the interfaces to stress corrosion cracking (i.e. inverse time-to-fracture) were found for the {122}, {111} and {113}, [110] symmetrical tilt grain boundaries, and for {015}, {013}, {012}, {025} and {037}, [100] symmetrical tilt grain boundaries [725, 728]. From

the point of view of the stress corrosion cracking, these grain boundaries are special. Note that the susceptibility cusps found for the [100] fit well with the minima of absolute values of the standard enthalpy of solute segregation for the symmetrical [100] tilt grain boundaries in bcc Fe−Si alloys [542] and this anisotropy well correlates with the structural dependence of the grain boundary energy [725].

Intergranular stress corrosion cracking of polycrystalline 304 austenitic stainless steel containing a distribution of general, low-energy and twin boundaries showed that $\Sigma = 3$ are more crack-resistant interfaces compared to other special grain boundaries (Σ=9 and Σ=27) [726]. The main reason for this degradation is chromium depletion of the grain boundaries of sensitised steels [729]. 3D characterisation of polycrystalline austenitic stainless steel enabling to determine the orientation of the grain boundary planes showed that the majority of the grain boundaries found on the fracture surface were characterised by high $\{hkl\}$ index planes: If there was present a low-index grain boundary, it failed in a ductile manner. This is direct proof of the resistance of individual grain boundaries to intergranular stress corrosion cracking and their role in crack-bridge development [730].

Classical experiments of Gleiter et al. [731, 732] with the corrosion remove of small single-crystalline spheres produced of copper or silver containing either 10^{-1}% of bismuth or units of percents of gold, from the single-crystalline plate under ultrasonic irradiation in a bath of demineralised water can also be considered as example of the stress corrosion cracking. These experiments revealed that only the grain boundaries between the spheres and the plate exhibiting special orientation relationship remained untouched by corrosion while the spheres arranged in a general relationship were removed under the above treatment. The results well prove the close relationship between the strength of the grain boundaries and the level of bismuth segregation [731, 732].

The effect of the grain boundary structure in intergranular stress corrosion cracking was also documented for example of a pipeline steel. Low-angle and special grain boundaries are more crack-resistant than general grain boundaries and the crack initiation and propagation of intergranular stress corrosion cracking is suppressed in material with large portion of special and low-angle grain boundaries. It also means that the strength of the texture of the material enhances its cohesion [733].

The intergranular stress corrosion cracking was found to propagate predominantly along general grain boundaries of 304L type austenitic stainless steels. If the portion of the general grain boundaries was reduced by thermomechanical treatment, the initiation and propagation of the intergranular stress corrosion cracking was substantially suppressed [734]. Although stress corrosion cracking of this alloy can be promoted by grain boundary segregation of phosphorus, it seems that this segregation alone is not sufficient to cause intergranular stress corrosion cracking [735]. The effects of decarburisation on the grain boundary segregation of phosphorus and primary water stress corrosion cracking have been investigated in a low-alloy steel. After decarburisation at 900°C, the low-alloy steel showed intergranular brittleness, arising from phosphorus segregation at grain boundaries. A drastic decrease in intergranular fracture strength was observed with increasing

grain boundary concentration of phosphorus, e.g. 610 MPa after decarburisation alone and 320 MPa after subsequent holding at 490°C for 10 days. Oxide films to the depths of about 80 μm were formed along the grain boundaries of the decarburised surface region and, at slower strain rate, these acted as pre-cracks for intergranular stress corrosion cracking in a primary water environment [736].

High-resolution analytical electron microscopy study of stress corrosion cracking of 316 austenitic stainless steel and nickel-based alloy 600 revealed that active segregation and precipitation play a major role in this process. This is documented by presence of deeply attacked grain boundaries outside the main crack. The attacked grain boundaries contained layers of oxides maximum 10-nm thick indicating the role of the grain boundary character and water chemistry. Impurities (lead) were found in a nanometre wide layer along the grain boundaries are involved in the stress corrosion cracking process [214]. The stress corrosion cracking of nickel-based superalloys is also promoted by phosphorus segregation at and chromium depletion from the grain boundaries [737]. Austenitic stainless steels and nickel-based alloys exhibit generally greater susceptibility for intergranular stress corrosion cracking than ferritic/martensitic alloys [738]. Decarburisation of a low-alloy steel results in enhanced grain boundary segregation of phosphorus and consequently, in increased intergranular stress corrosion cracking in water. Under such conditions, the strength of the material was reduced by factor approximately 2, that is from 610 to 320 MPa after decarburisation. As a result of the corrosion attack, the oxide films were found along the grain boundaries [736].

Intergranular stress corrosion cracking can be also promoted by the segregation effects at the grain boundaries induced by irradiation, such as enrichment of nickel or depletion of chromium. However, quantitative relationship between radiation-induced segregation and intergranular stress corrosion cracking of the materials has not been derived till now [739].

7.3 Grain Boundary Diffusion

Grain boundary diffusion is the movement of atoms along the grain boundaries under a driving force, which is mainly the difference in chemical potentials. In case of different solute and matrix atoms, it induces concentration changes at the grain boundary and therefore, is in close relationship to the grain boundary segregation. Let us now give the brief description of this phenomenon with focus to its relationship to grain boundary segregation.

7.3.1 Fundamentals of Grain Boundary Diffusion

The description of grain boundary diffusion is usually based on classical Fisher model [740, 741]. The grain boundary Φ is represented by a uniform and isotropic slab of the thickness, δ, characterised by high diffusivity, D_I^{Φ}, that is embedded in an isotropic crystal perpendicular to its surface with low diffusivity, $D_I \ll D_I{}^{\Phi}$

(Fig. 7.7a). Before the diffusion measurements, a layer of the solute or of the isotope of the same material is put at the surface. During annealing of such system at a constant temperature T for a time t, the atoms diffuse from the surface into the material. This diffusion occurs in two ways (a) via the volume diffusion into the grains and (b) via the grain boundary diffusion along the interfaces. Since $D_I \ll D_I^{\Phi}$, the grain boundary diffusion is much faster. The atoms moving along the grain boundary may either continue in the grain boundary diffusion or to diffuse perpendicularly to the interface into the grain regions adjacent to the boundary. As a result, a zone of the volume diffusion occurs in vicinity of the boundary. Mathematically, this complex diffusion is described by a set of two coupled equations,

$$\frac{\partial X_I}{\partial t} = D_I \left(\frac{\partial^2 X_I}{\partial x^2} + \frac{\partial^2 X_I}{\partial y^2} \right), \tag{7.10}$$

if $|x| > \delta/2$, and

$$\frac{\partial X_I^{\Phi}}{\partial t} = D_I^{\Phi} \frac{\partial^2 X_I^{\Phi}}{\partial y^2} + \frac{2D_I}{\delta} \left(\frac{\partial^2 X_I}{\partial x^2} \right) \tag{7.11}$$

for $x = \delta/2$. In (7.10) and (7.11), $X_I(x, y, t)$ is the bulk concentration of the solute and $X_I^{\Phi}(y, t)$ is its grain boundary concentration. The solution of (7.10) and (7.11) should fulfil certain surface conditions specified below and natural initial and boundary conditions at x and $y \to \infty$. A simple condition is keeping the constant source at the surface [740],

$$X_I(x, 0, t) = X_{I,0} = \text{const.} \tag{7.12}$$

This condition can be established by depositing a thick surface layer of the solute, the thickness h of which exceeds the diffusion path, $h \gg (Dt)^{1/2}$. Presently, more frequently used experiments are performed with $h \ll (Dt)^{1/2}$. Therefore, another condition of so-called instantaneous source or thin layer should be applied,

$$X_I(x, y, 0) = M\delta_{\mathrm{D}}(y) \quad \text{and} \quad (\partial X_I/\partial y)_{y=0} = 0. \tag{7.13}$$

In (7.13) M is the amount of the solute per unit area deposited at the surface, and δ_{D} is the Dirac delta-function. This condition suggests that the initial layer of the solute is completely consumed by the specimen during the diffusion experiment.

The relationship between functions $X_I(x, y, t)$ and $X_I^{\Phi}(y, t)$ depends on both the character of the diffusing species (self-diffusion or impurity diffusion) and the type of the matrix material (pure metal or alloy). In case of the impurity diffusion in a pure metal, which is interesting from the point of view of the grain boundary segregation, the condition involves the equilibrium segregation factor s[1]

$$X_I^{\Phi}(y, t) = sX_I(y, t) \tag{7.14}$$

[1] Let us note that he segregation factor s is identical to the grain boundary enrichment ratio β_I^{Φ} defined by (4.19).

which is independent of both, y and t. This equation reflects two assumptions (a) the impurity atoms in the grain boundary are in local thermodynamic equilibrium with the atoms in the lattice adjacent to the boundary, that is the grain boundary segregation is locally at equilibrium at any depth; and (b) the grain boundary segregation follows the relationship $X_I^{\Phi} = sX_I$ supposing s is the function of temperature only. Indeed, this relationship only holds when both X_I^{Φ} and X_I are small enough, so that the thermodynamic activities of the solute in the grain boundary and in the bulk are proportional to the respective concentrations (Henry law). Another interesting situation is the grain boundary self-diffusion in concentrated alloys [742, 743]. If the grain boundary diffusion of the tracer B* in a binary A–B alloy occurs, (7.14) can be applied supposing (a) an equilibrium grain boundary segregation of B establishes before and persists during the diffusion annealing; (b) the amount of B* diffused into the sample is very small and does not affect the distribution of component B in the sample; and (c) the isotope equilibrium with respect to B is established between the grain boundary and the adjacent lattice at any depth. The factor s in (7.14) equals to the ratio $X_{\mathrm{B}}^{\Phi}/X_{\mathrm{B}}$ of the corresponding net concentrations of B. This ratio characterises the equilibrium grain boundary segregation in the alloy. Let us mention that the concentrations of B do not need to be small and the grain boundary segregation can be either in the linear (Henry) type or in the saturation regime.

Let us now focus to the measurements of the grain boundary diffusion. The majority of these experiments are carried out using radiotracers and the serial sectioning technique [743]. After the deposition and the diffusion annealing, the concentration of the isotope is measured in removed thin layers of the material parallel to the surface (e.g. mechanically) using a crystalline γ-detector or a liquid scintillation counter. In this way, the average layered concentration of the diffusant, $\bar{c}$, is measured in dependence on the penetration depth y (Fig. 7.7b). If the concentration profile calculated using the exact analytical solution [744] is plotted as $\log \bar{c}$ vs. y^n, it results in an almost straight line for $n = 6/5$ [745, 746]. Further, the linear

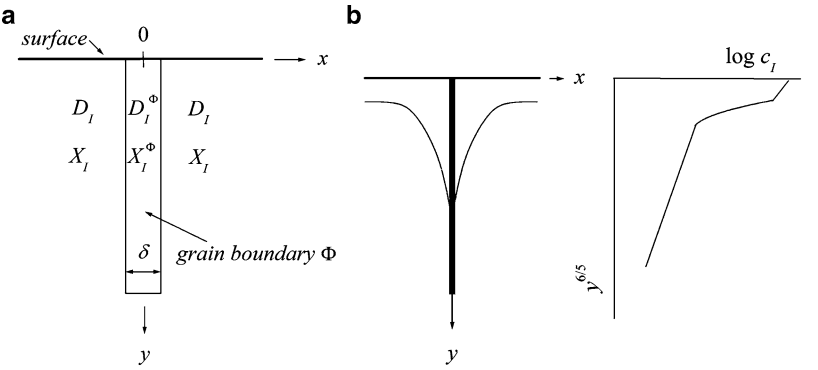

Fig. 7.7 Schematic representation of the grain boundary diffusion (**a**) geometry; (**b**) penetration profile. If $a \ll 1$ and $\beta \gg 1$ (cf. (7.17) and (7.18)), the tail of the profile is a straight line in the coordinates $\log \bar{c}$ vs. $y^{6/5}$ (according to [740])

part of the profile varies with the reduced depth ω,

$$\omega = \frac{y}{\sqrt{s\delta D_I^{\Phi}}} \left(\frac{4D_I}{t} \right)^{1/4} \tag{7.15}$$

with approximately constant slope $-\partial \ln \bar{c} / \partial y^{6/5} \approx 0.78$. Knowing the slope of the linear part of the profile, one can thus calculate the product $s\delta D_I^{\Phi}$ as

$$s\delta D_I^{\Phi} = 1.322 \sqrt{\frac{D_I}{t}} \left(\frac{\partial \ln \bar{c}}{\partial y^{6/5}} \right)^{-5/3} \tag{7.16}$$

for constant source. The volume diffusion coefficient D_I is supposed to be known from independent measurements. The application of (7.16) is only possible if the following conditions are fulfilled (a) the parameter β (here the Le Claire parameter) [747] defined as

$$\beta = \frac{s\delta D_I^{\Phi}}{2D_I \sqrt{D_I t}} \tag{7.17}$$

must be large, $\beta > 10$; and (b) the parameter α defined as

$$\alpha = \frac{s\delta}{2\sqrt{D_I t}} \tag{7.18}$$

must be small, $\alpha < 0.1$.

The product $s\delta D_I^{\Phi}$ can be also determined from the linear part of the plot $\log \bar{c}$ vs. y^n, in case of an instantaneous source where $-\partial \ln \bar{c} / \partial y^{6/5} \approx 0.775$, and for $\alpha < 0.1$ and $\beta > 10^4$

$$s\delta D_I^{\Phi} = 1.308 \sqrt{\frac{D_I}{t}} \left(\frac{\partial \ln \bar{c}}{\partial y^{6/5}} \right)^{-5/3}. \tag{7.19}$$

The numerical constant in (7.19) should be slightly modified for $\beta < 10^4$ [748].

Only one part of the profile dominated by the grain boundary diffusion is considered in these relations although the penetration profile has two parts as shown schematically in Fig. 7.7b. In the surface region, the volume diffusion runs from the surface. This part can be used for evaluation of the coefficient of volume diffusion. On the other hand, the region far from the surface involves simultaneous grain boundary and lateral volume diffusion from the boundary to the adjacent grains. This profile should become a straight line of the $\log \bar{c}$ vs. $y^{6/5}$ dependence and its slope can be then used to determine the grain boundary diffusivity.

Equations (7.16) and (7.19) are used to correlate the results of the grain boundary diffusion measurements and provide us with the product $s\delta D_I^{\Phi}$. Individual values of s, δ and D_I^{Φ} remain unknown. The assumption that $\delta = 0.5$ nm is a good approximation [740]. In the diffusion studies under the condition of the dilute limit, it is

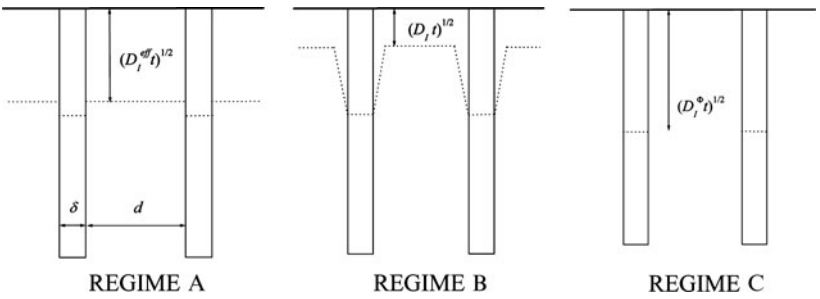

Fig. 7.8 Schematic representation of regimes A, B and C of the diffusion kinetics in system containing grain and grain boundaries (according to [740])

possible to distinguish so-called A, B and C kinetic regimes of the diffusion process as measured on identical polycrystalline material [746] (Fig. 7.8).

The *A regime* is observed in the limiting case combining the conditions of high temperatures, very long annealing periods and small grain sizes d. In such conditions, the volume diffusion length, $(D_I t)^{1/2} \gg d$, and the volume diffusion dominates, although the grain boundary diffusion also occurs, which affects the total measured concentrations in different depths beneath the surface thus providing an effective diffusion coefficient D_I^{eff} according to the Fick law (Fig. 7.8).

At lower temperatures, shorter annealing periods and/or larger grain size than that applied in A regime, the diffusion exhibits so-called *B regime*. In this regime, the diffusion length should fulfil the condition $s\delta \ll (D_I t)^{1/2} \ll d$. It means that the grain boundary diffusion takes place simultaneously with the volume diffusion but in contrast to A regime individual grain boundaries are far from each other so that the expressions derived for an isolated grain boundary are valid. The condition for B regime implies $\alpha \ll 1$ and $\beta \gg 1$ supposing much deeper penetration of the solute along the grain boundaries compared to the volume [746]. Then, the penetration profile has a two-step shape shown schematically in Fig. 7.8b. The part of the profile related to the grain boundary diffusion depends on the dimensionless variable ω only defined by (7.15) suggesting the quasi-steady character of the grain boundary diffusion [748]. The triple product $s\delta D_I^{\Phi}$ is the only quantity that can be determined in B regime according to (7.16) and (7.19). B regime is the most commonly used for the measurements of grain boundary diffusion.

Much lower temperatures and/or shorter annealing times than applied in regime B result in almost "freezing" of the volume diffusion and in domination of the grain boundary diffusion without any essential leakage to the volume (Fig. 7.8c). This regime is called *C regime* and it is controlled by the condition $(D_I t)^{1/2} \ll s\delta$. Consequently, $a \gg 1$ (practically starting from $\alpha > 10$). The concentration profile in this regime is either a Gaussian function (instantaneous source) or an error function (constant source) with the diffusion coefficient D_I^{Φ}. If the profile is measured experimentally, D_I^{Φ} can be determined separately from s and δ [740].

7.3.2 Relationship Between Grain Boundary Diffusion and Segregation

Because there appears the segregation factor s, which is nearly identical with the grain boundary enrichment ratio β^{Φ} (4.19) in the expressions describing grain boundary diffusion, the thermodynamic parameters of the grain boundary segregation can also be obtained from the diffusion experiments.

As was mentioned above, the studies of the grain boundary diffusion are most frequently performed in B regime and for determination of the diffusion parameters, (7.16) and (7.19) are applied. For impurity diffusion, this method only provides the triple product $s\delta D_I^{\Phi}$. While the grain boundary width, δ, can be approximated by a constant value $\delta = 0.5\,\text{nm}$, the grain boundary segregation factor s and the grain boundary diffusion coefficient D_I^{Φ} are still to be determined. Parameters s and D_I^{Φ} can be separated on basis of the measurements of the grain boundary diffusion in a wide temperature range under conditions of both B and C regimes, because C regime can directly determine D_I^{Φ}. Knowing the values of D_I^{Φ}, s can be determined from the values of the product $s\delta D_I^{\Phi}$ measured in B regime measurements as $s\delta = \left(s\delta D_I{}^{\Phi}\right)/D_I{}^{\Phi}$ [740].

The product $s\delta D_I^{\Phi}$ fulfils the Arrhenius law,

$$s\delta D_I^{\Phi} = \left(s\delta D_I^{\Phi}\right)_0 \exp\left(-\frac{Q_I^{\text{app}}}{RT}\right), \tag{7.20}$$

where Q_I^{app} is the apparent activation energy. Similarly, s is dependent on temperature. In the infinitesimal dilution limit when $X_I \ll X_I^{\Phi} \ll 1$,

$$s = s_0 \exp\left(-\frac{\Delta H_I^0}{RT}\right), \tag{7.21}$$

where ΔH_I^0 is the standard enthalpy of segregation. As D_I^{Φ} also follows the Arrhenius law, $D_I^{\Phi} = D_{I,0}^{\Phi} \exp\left(-H_I^{\Phi}/RT\right)$,

$$Q_I^{\text{app}} = H_I^{\Phi} + \Delta H_I^0. \tag{7.22}$$

If Q_I^{app} and H_I^{Φ} are determined from the diffusion measurements in B and C regimes, respectively, ΔH_I^0 can be obtained [740]. From the temperature dependence of D_I^{Φ}, the entropic contributions can also be obtained and similarly to ΔH_I^0, ΔS_I^0 can also be evaluated $\Delta S_I^0 = R \ln s_0$.

The possibility to determine the thermodynamic parameters of segregation from the measurements of grain boundary diffusion is very interesting. Despite the fact that two phenomena and thus their interaction can be studied simultaneously, it is possible to determine the thermodynamic parameters of the grain boundary segregation also for systems where other methods of interfacial analysis fail, such as AES or ESCA. This is especially important for non-brittle and less-segregating solutes.

Main problem is that the measurements in the C regime are extremely difficult and, therefore, they have been performed only rarely. Only recently, reliable and systematic measurements in the C regime have been facilitated by using of both the carrier-free radioisotope layers and the extremely sensitive detectors with a large counting efficiency and low background [749]. Up to now, combined measurements in B and C regime were realised in the systems such as tellurium [750], selenium [751] and nickel [752] in silver and gold [753], selenium [754] and silver [755] in copper.

In some systems at low temperatures, the grain boundary segregation is quite strong and the grain boundaries may reach their saturation with the solute. In this case, a non-linear relation between X_I^{Φ} and X_I is observed, that is $s \neq$ const. It means that X_I^{Φ} changes with the changes of the depth y. The dependence of X_I^{Φ} on y may alter the shape of the profile. In this case, Langmuir–McLean segregation isotherm (4.61) should be used instead of the linear relationship between X_I^{Φ} and X_I, that is the conditions of the Henry law is no more fulfilled. This replacement causes slight changes of the concentration profiles. Just below the surface, a saturation region of the grain boundary exists in which $\bar{c}$ rapidly decreases with ω and the profile has a strong upward curvature because $X_I^{\Phi} \approx 1$ while X_I rapidly reduces. Under the saturation layer, the region of linear segregation region ($\omega > 1$) exists where the profile is linear with ω because both X_I^{Φ} and X_I are small and the Henry isotherm is a good approximation. This part of kinetics can be used for determination of $s\delta D_I^{\Phi}$ [740]. For example, this situation arises in case of silver segregation in copper [754,755]. From this type of measurement, the segregation energy (enthalpy) of silver in copper was determined to be $-29 \pm 13\,\mathrm{kJ/mol}$. This value is in good agreement with the AES data, $\Delta H_{\mathrm{Ag}} \geq -40\,\mathrm{kJ/mol}$ [756].

To obtain reliable results on grain boundary diffusion, appropriate measurements have to be performed at relatively high temperatures. In case of very pure polycrystalline metals with soluble solutes, recrystallisation or grain growth can occur during annealing the samples. Then the effect of moving grain boundaries must be taken into account. Non-linear segregation of poorly soluble elements like silver or iron in copper leads to strong curving the diffusion profiles which can be effectively used as a tool to measure segregation enthalpies in grain boundaries. Even in these cases, however, quantitative analysis of heterodiffusion profiles shows that grain boundary diffusion remains one of the best ways to obtain information on grain boundary chemistry [743].

The values of the standard enthalpy and entropy of grain boundary segregation determined on basis of the diffusion experiments are also included in Appendix A.

7.4 Grain Boundary Engineering

The knowledge of structural dependence of various grain boundary phenomena including solute segregation can also be used in practice for production of polycrystalline materials with optimum properties. As shown for many examples throughout

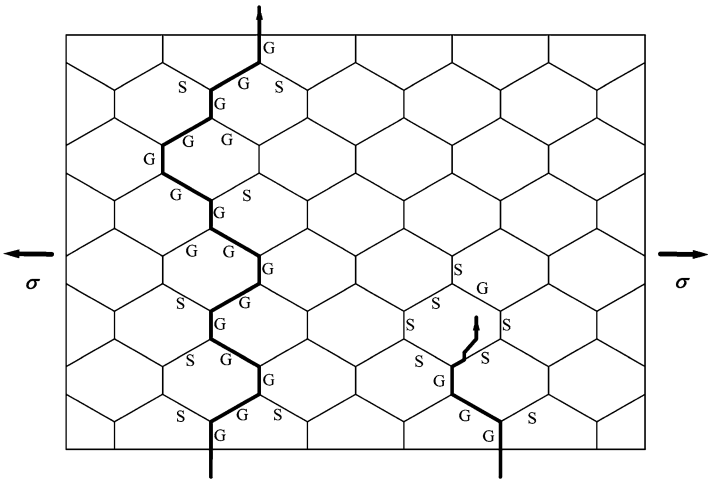

Fig. 7.9 Schematic representation of the fracture in a polycrystalline material. The continuous path of general grain boundaries (*left side*) facilitates an easy fracture. On the other hand, the fracture along the path containing special grain boundaries interrupting the network of general interfaces (*right side*) is more difficult and needs larger stress and/or the material fractures in transcrystalline manner (According to [32])

this book, the behaviour of special and general grain boundaries differs substantially in many cases. One very important property is brittle fracture.

As mentioned above, the highly segregated general grain boundaries are more prone to intergranular brittle fracture than the special interfaces [757]. It means that the brittle separation of a polycrystalline material under stress will proceed preferentially along the general interfaces. If the general grain boundaries form a continuous path throughout the material (left side of Fig. 7.9), relatively low applied stress can cause this separation. If however, the path of the general grain boundaries is interrupted by special grain boundaries (right side of Fig. 7.9), the brittle fracture is not so easy as in previous case. To crack such material it is necessary to increase the stress and then, the fracture will also proceed in transrystalline manner. It follows from this consideration that the properties of a polycrystal will depend on the character and distribution of individual grain boundaries in the polycrystal. Watanabe [32] formulated the concept of the Grain Boundary Design of polycrystalline materials, the basic idea of which is to design and produce the polycrystalline material through controlling the distribution of the types of the grain boundaries in order to obtain polycrystalline materials with desirable properties and performance. At present, this concept is widely known as *grain boundary engineering (GBE)*.

Successful GBE is based on detail knowledge of the properties of individual grain boundaries. However, a polycrystalline material contains huge number of grain boundaries interconnected with each other. A small piece of polycrystal of the size of $1\,\mathrm{cm}^3$ with the average grain size of 0.1 mm in diameter contains 10^6 grains, each of them surrounded by 8–12 grain boundaries! It is clear that the design of the

Table 7.2 Grain boundary control applicable to grain boundary engineering [759]

Phenomenon	Controlling parameter	Application
Grain boundary density	Grain size, grain boundary volume	Enhancement of strength and ductility, new properties
Grain boundary geometry	Grain boundary inclination, dihedral angle	Enhancement of creep ductility and superconductivity
Grain boundary morphology	Precipitate shape, size and density	Enhancement of corrosion resistance and ductility
Grain boundary chemistry	Segregation level, width of precipitate-free zone	Reduction of embrittlement, enhancement of corrosion resistance
Grain boundary structure	Grain boundary type and character distribution	Enhancement of strength and ductility, new properties

polycrystalline material and the manipulation with the grain boundaries is extremely complicated even in such a small piece of material. We must take into account that the grain boundaries are buried in the material and adjustment of a grain boundary to a desirable orientation may mean simultaneous change of the character of other boundaries of this single grain. In addition to structural parameters of grain boundaries, such as their character, structure and connectivity, there are many possible parameters that have to be considered for successful GBE. Geometrical parameters (grain size and shape, boundary area, boundary junctions), morphological parameters (boundary inclination and faceting, grain boundary phases, grain boundary width), composition parameters (grain boundary segregation and precipitation) and energetic parameters (grain boundary energy, electronic charge and magnetic state) belong among them [758]. In Table 7.2, the types of the grain boundary phenomena, controlling parameters and applications for the improvement of material performance are listed.

Besides all above-mentioned phenomena and parameters affecting the structure of the planned polycrystal, it is also necessary to consider formation of new recrystallised grain boundaries and their migration. In this way, the initially formed grain boundaries may change their structure and thus energy and migration characteristics. These processes can substantially control the micro-structure of the polycrystal during recrystallisation and following grain growth [758, 760].

One of the most important features necessary for successful GBE is the grain boundary classification, that is the specification of the grain boundary type, because the portion of the special grain boundaries is decisive for the properties of optimised polycrystal. As the low value of Σ is the simplest geometric characteristics for the special grain boundaries, the CSL concept is widely used for characterisation of the grain boundaries and increased portion of low-Σ grain boundaries is a measure of improved polycrystal [759–761]. The low-Σ grain boundaries can also well multiply at the triple junctions. If the frequency of $\Sigma = 3$ grain boundaries is high, their meeting in the grain boundary triple junctions, namely results in the so-called multiple twinning, which seems to be a key factor of GBE in materials with low value of stacking fault energy. Such multiple twinning can be represented either by

joining or by dissociation [762],

$$\Sigma A + \Sigma B \rightarrow \Sigma(A \times B) \quad \text{or} \quad \Sigma A + \Sigma B \rightarrow \Sigma(A/B). \tag{7.23}$$

The relationship on the right-hand side of (7.23) is valid if A/B is an integer and A > B. Therefore, if two $\Sigma = 3$ grain boundaries meet at the triple junction, a $\Sigma = 9$ grain boundary occurs, and if $\Sigma = 3$ and $\Sigma = 9$ grain boundaries meet there, the resulting one is either another $\Sigma = 3$ or $\Sigma = 27$ [762].

Anisotropy of grain boundary segregation affects strongly many properties and processes occurring in polycrystals, for example grain boundary energy and mobility. In this way, the grain boundary character distribution will also be affected by presence of solutes and impurities. For example, increased bulk concentration of sulphur in pure nickel from 3×10^{-1} ppm to 10 ppm reduces the portion of the $\Sigma = 3$ grain boundaries from more than 90% to about 55% (Fig. 7.10) [757]. Similarly, increasing bulk concentration of sulphur in α-iron reduces the fraction of special grain boundaries. Sulphur is active in this sense only in the absence of carbon: Under presence of carbon, the frequency of appearance of special grain boundaries remains similar to that observed in pure iron [763]. The existence of the compensation effect (cf. Chap. 5) and its consequence in reversing the type of anisotropy of grain boundary properties (e.g., the mobility [48] and solute segregation [566]) can also strongly affect the mechanism of formation of the structure and the final distribution of the grain boundaries.

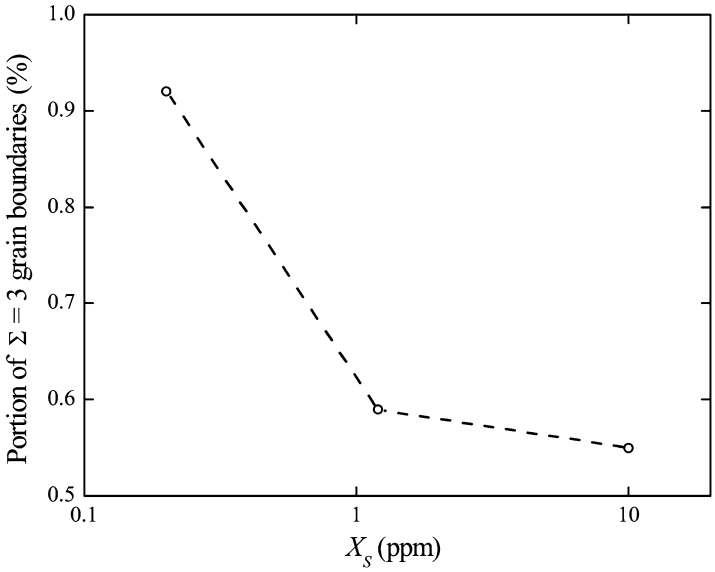

Fig. 7.10 Dependence of the portion of $\Sigma = 3$ grain boundaries in pure nickel on the bulk concentration of sulphur (according to [757])

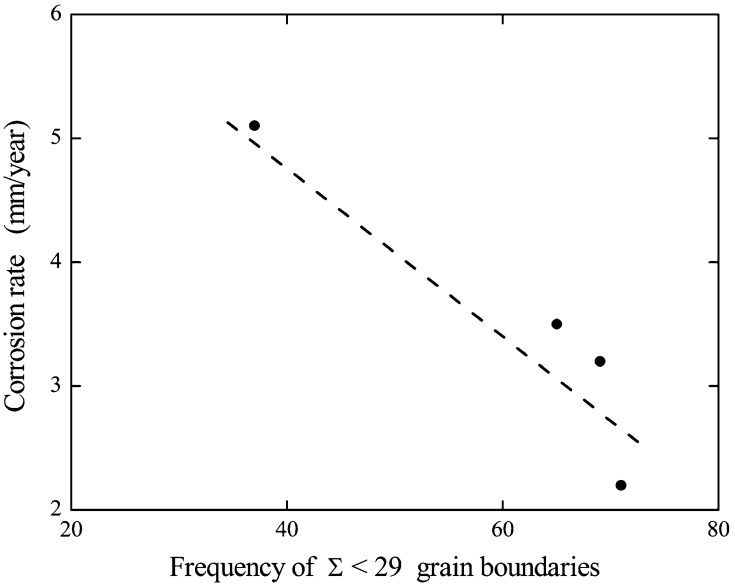

Fig. 7.11 Dependence of the rate of grain boundary corrosion in a nickel-based alloy on the frequency of $\Sigma < 29$ grain boundaries. According to [768]

In many cases, a correlation between the density of low-Σ grain boundaries and improved properties of materials are reported. For example, the ductility of an Fe−6.5mass.%Si alloy [764] and boron-free Ni_3Al [765] was enhanced when the portion of low-Σ grain boundaries was substantially increased. Optimisation of the grain boundary character distribution can improve the superplasticity in an Al−Li alloy [766] or magnetostriction-induced strain and shape memory effect in an Fe−Pd alloy [574]. Increased frequency of low-Σ grain boundaries in 304 austenitic stainless steel suppressed boron segregation and carbide precipitation at grain boundaries [767] and suppressed grain boundary corrosion in a nickel-based alloy [762, 768] as is shown in Fig. 7.11. Corrosion and growth resistance of positive grids used in lead-acid batteries was increased by 20 and 75%, respectively, by increasing the portion of the CSL grain boundaries from 12 to more than 65% [769].

As was already mentioned in Chap. 2, the CSL approach reflects only the three DOFs related to the misorientation of the two adjoined grains but does not specify directly the crystallography of the boundary plane itself [769, 770]. It was already shown for many examples that the grain boundary plane orientation plays an important role in grain boundary classification. As mentioned above, the study of solute segregation at individual grain boundaries in a carefully chosen set of bicrystals of an Fe−Si alloy suggests that there should exist at least one special grain boundary for any misorientation of the two grains that is characterised by low-index plane [94, 100, 762, 771]. In case of pure nickel, it was shown that only 2/3 of $\Sigma = 3$ and $\Sigma = 9$ grain boundaries possessed "special" orientation in a polycrystal [772]. This

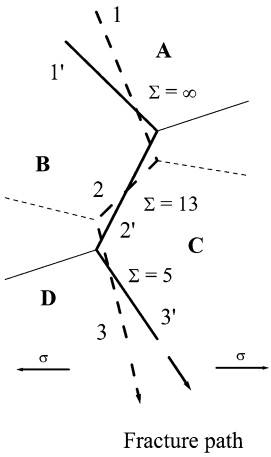

Fig. 7.12 Model ensemble of four grains, A, B, C and D, with mutual orientation relationships A–B: 45°[100], B–C: 22.6°[100], and C–D: 36.9°[100]. Two alternative fracture paths (occurring under stress σ) along grain boundaries are depicted (**a**) 1–2–3, formed by general interfaces $\{0k_s l_s\}$, (023)/(015) and (0 1 14)/(0 20 23) (*full-line path*), and (**b**) $1'$–$2'$–$3'$ formed by special interfaces (001)/(011), {015} and {013} (*dashed-line path*). Two configurations are inclined by 22.5°[100]. According to [94]

idea modifies the approaches to the technologies of production of polycrystals with optimum properties in GBE: It is not necessary to consider exclusively the reorientation of the grains constrained in the material during recrystallisation or to locally deform the lattice but additionally, also to take into account the grain boundary reorientation during grain growth when the interface inclines into an energetically advantageous special orientation [94, 100, 773, 774]. This is schematically shown in Fig. 7.12 [94, 100]. It is obvious that the grain boundary inclination is much easier to be realised compared to the rotation of individual grains buried in a polycrystalline material.

Let us mention for completeness that in the GBE one has to deal not only with grain boundaries alone. They are constrained in triple junctions of three interfaces or quadruple points of four grain boundaries. The chemistry of these features as well as their migration ability is presently under intensive investigation. Similarly to grain boundaries, the triple junctions exhibit the segregation effects [195]. The importance of the triple junctions led to formulation of an alternative approach to the GBE: the grain boundary junction engineering [774, 775].